Electrical Power and Energy Systems 139 (2022) 107992

Contents lists available at ScienceDirect

International Journal of Electrical Power and Energy Systems

journal homepage: www.elsevier.com/locate/ijepes

Envisioning security control in renewable dominated power systems through stochastic multi-period AC security constrained optimal power flow

Mohammad Iman Alizadeh, Muhammad Usman, Florin Capitanescu *

Luxembourg Institute of Science and Technology (LIST), Environmental Research and Innovation (ERIN) Department, 41-rue du Brill, L-4422 Belvalux, Luxembourg

ARTICLE INFO

Keywords:
Congestion management
Energy storage systems
Flexibility
Flexible loads
Security-constrained optimal power flow
Voltage control

ABSTRACT

The accelerated penetration rate of renewable energy sources (RES) brings environmental benefits at the expense of increasing operation cost and undermining the satisfaction of N-1 security criterion in transmission systems. To address the latter issue, this paper envisions N-1 security control in RES dominated power systems through stochastic multi-period AC security constrained optimal power flow (SCOPF). The paper extends the state-of-the-art, i.e. deterministic and single time period AC SCOPF, to capture two new dimensions, RES stochasticity and multiple time periods, as well as emerging sources of flexibility such as flexible loads (FL) and energy storage systems (ESS). Accordingly, the paper proposes and solves for the first time a new problem formulation in the form of stochastic multi-period AC SCOPF (S-MP-SCOPF). The S-MP-SCOPF is formulated as a non-linear programming (NLP) problem. It computes optimal setpoints of flexibility resources and other conventional control means for congestion management and voltage control in day-ahead operation. As another salient feature, the proposed model is comprehensive and accurate, using: AC power flow model for both pre-contingency and post-contingency states, inter-temporal constraints for resources such as FL and ESS in a 24-hours time horizon and RES uncertainties. The importance and performance limitation of the proposed model through a direct approach, pushing the problem size up to the solver limit, are illustrated on two test systems of 5 nodes and 60 nodes, respectively. For the 60 node test system, the largest successful case can manage 30 scenarios and is solved in 22,110 s. Future work will develop a tractable solution algorithm.

1. Introduction

1.1. Motivation

To attain the stringent sustainable goals set to them, power systems worldwide are hosting increasingly large amounts of variable renewable energy sources (RES), mainly wind and solar, at all voltage levels. However, massive RES penetration significantly challenges the enforcement of transmission system security [1] due to the inherent variability and difficulty to predict RES output. In this context, power systems operate closer to their security limits and hence fulfilling N-1 security becomes a challenging task, particularly under stressed operation conditions, unexpected RES output, and/or unavailability of effective control actions. Regarding the latter aspect, as classical control means (e.g., conventional power plants) and controllable RES may not be sufficient to fulfil security, additional emerging sources of flexibility, such as flexible loads (FL) and energy storage systems (ESS), are being deployed to enhance power system flexibility and offset issues provoked by RES [2,3]. Deterministic AC security-constrained optimal power flow (SCOPF) [4–6] is the conventional tool to enforce N-1 security at a given period of time and is mainly used in the day-ahead operation for the cost-optimal procurement of ancillary services (e.g., for managing congestion and voltages). To this end, SCOPF computes the optimal balance of preventive (i.e., pre-contingency) and corrective (i.e., post-contingency) actions able to guarantee static system security (i.e., pertaining to congestion and voltage magnitude) for a set of postulated (e.g., N-1) contingencies. Lastly, SCOPF problems, in their simplest form, are formulated as large scale (non-convex) non-linear programs (NLPs) whose main difficulty lie in their large problem size [4–6]. A brief yet comprehensive overview of SCOPF problems [7,8] that are published in the literature is presented in the next section.

1.2. Related works

Deterministic single period AC SCOPF is state-of-the-art [9–16]. Its solution has been extensively explored through various algorithms:

* Corresponding author.
E-mail address: fcapitanescu@yahoo.com (F. Capitanescu).

https://doi.org/10.1016/j.ijepes.2022.107992
Received 31 August 2021; Received in revised form 16 December 2021; Accepted 21 January 2022
Available online 11 February 2022

Nomenclature

Sets

E	Set of ESS indexed by e
F	Set of FL indexed by f
G	Set of generators indexed by g
K	Set of operation states, including normal and contingencies, indexed by k
N	Set of nodes indexed by n
R	Subset of nodes with RES
S	Set of scenarios indexed by s
T	Set of time periods indexed by t

Parameters

ΔP_{G_g}	ramp rate limit of generator g
ΔT	time interval ratio
$\eta^{ch,e}$	charging efficiency rate of ESS e
$\eta^{dis,e}$	discharging efficiency rate of ESS e
$\overline{P}_e^{ch}/\overline{P}_e^{dis}$	maximum active power charging/discharging limit of storage e
$\overline{P}_f^{inc}/\overline{P}_f^{dec}$	maximum active power increase/decrease limit of FL f
π_s	probability of occurrence of scenario s
$\underline{P}_g/\overline{P}_g$	minimum/maximum active power limit of generator g
$\underline{Q}_g/\overline{Q}_g$	minimum/maximum reactive power limit of generator g
$\underline{V}_n/\overline{V}_n$	minimum/maximum voltage limit at node n
B_{nm}^{sh}	shunt susceptance of the branch linking nodes n and m
B_{nm}	susceptance of the branch linking nodes n and m
c_e	cost (€/MWh) of active power of energy storage e
c_f	cost (€/MWh) of active power of flexible load f
c_g	cost (€/MWh) of active power re-dispatch of generator g
c_n^{Gcurt}	cost (€/MWh) of active power curtailment at node n
c_n^{Lcurt}	cost (€/MWh) of active load curtailment at node n
G_{nm}	conductance of the branch linking nodes n and m
$I_{nm}^{\max}$	maximum current of line linking nodes n and m
$P_{D_{n,t}}$	load active power at node n, period t
$P_{G_{g,t}}^{*}$	active power of generator g at time t cleared in the energy market
$Q_{D_{n,t}}$	load reactive power at node n, period t
$R_{n,s,t}$	RES active power at node n, period t, scenario s
$SOC_e^{\max}$	maximum State-of-Charge for storage e
$SOC_e^{\min}$	minimum State-of-Charge for storage e

Variables

$e_{n,s,t}^k$	real part of complex voltage $\left(e_{n,s,t}^k + jf_{n,s,t}^k\right)$ at node n, period t, scenario s, state k
$f_{n,s,t}^k$	imaginary part of complex voltage at node n, period t, scenario s, state k
$Lc_{n,s,t}^k$	active load curtailment at node n, time t, scenario s, state k
$P_{e,s,t}^{ch,k}$	active power charging of storage e at time t, scenario s, state k
$P_{e,s,t}^{dis,k}$	active power discharging of storage e at time t, scenario s, state k
$P_{f,s,t}^{dec,k}$	active power decrease of FL f at time t, scenario s, state k
$P_{f,s,t}^{inc,k}$	active power increase of FL f at time t, scenario s, state k
$P_{G_{g,s,t}}^k$	active power of generator g at time t, scenario s, state k
$P_{inj_{n,s,t}}^k$	active power injection at node n, time t, scenario s, state k
$Q_{c_{n,s,t}}$	reactive load curtailment at node n, time t, scenario s, state k
$Q_{G_{g,s,t}}^k$	reactive power of generator g at time t, scenario s, state k
$Q_{inj_{n,s,t}}^k$	reactive power injection at node n, time t, scenario s, state k
$Rc_{n,s,t}^k$	active power of RES curtailment at node n, time t, scenario s state k
$SOC_{e,s,t}^k$	State-of-Charge for storage e at period t, scenario s, state k

decomposition methods (e.g., Benders decomposition or iterative algorithms based on contingencies filtering, both embedding interior-point method for core NLP problem) applied to exact formulations [9–12], approximations [10,13], meta-heuristics [14] and convex relaxations (e.g., semi-definite programming [9,15] and second order cone programming [16]) that are able to assess the optimality gap of exact algorithms' solution. Further modelling advancement regarding generators' response after contingencies to frequency and voltage control have been also explored [13,17].

Solving deterministic single period AC SCOPF is today computationally demanding but still scalable to systems of reasonably large size (i.e., thousand nodes) [6]. Despite AC SCOPF is the state-of-the-art, some works develop sophisticated algorithms for its linear (DC) SCOPF approximation via column and constraint generation [18], constraints redundancy screening [19], alternating direction method of multipliers (ADMM) in a distributed manner [20], network compression [21], linearized AC SCOPF [22], and machine learning [23].

To capture RES inherent variability, two timely extensions of SCOPF have also been developed independently to address:

- *uncertainties* (regarding RES) based on robust optimization [24], distributionally robust optimization [25], stochastic optimization (exact [26], simplified DC [27] or relaxed [28]) and chance-constrained optimization [29]; other uncertainties (e.g., regarding corrective control potential failure) were tackled via chance-constraints [30] or DC model using ADMM regarding demand uncertainties [31] .
- *multiple time periods* (linked by inter-temporal constraints) via the simplified DC model [8,32] or the exact AC model [33,34] .

However, these extensions are very scarce and tremendously increase the computational burden of the problem.

Table 1
Model features of various approaches.

Model	Deterministic single-period	Multiple time periods	Operation uncertainty	Flexibility resources	AC model	Scalability
[9–18]	x				x	x
[19],[23]	x					x
[20]	x					
[24]			x		x	
[25]			x			x
[26]		x		x		
[27]			x			x
[28]			x		x	
[29]			x		x	
[30]			x		x	
[8]		x	x			x
[32]		x	x	x		x
[33]		x				
[34]		x			x	
proposed		x	x	x	x	

Additionally, to reliably deal with RES variability, a meaningful SCOPF problem should also consider time dependent emerging flexibility resources (e.g., FL and ESS). However, these flexibility resources were considered only sporadically and in a single period deterministic SCOPF [35].

1.3. Contributions and paper organization

It can be concluded that the approaches aimed to extend SCOPF state-of-the-art are not only very scarce but also have considered separately the two main features: RES uncertainties and multiple time periods. In addition, the approaches to any of these two challenges do not model in a joint fashion the two other difficult features such as AC network model and emerging flexibility resources.

To bridge this gap, as a conceptual contribution, this paper proposes the new envisioned concept of multi-period AC SCOPF under uncertainties to control N-1 security in RES-dominated power systems of the future. *The main contribution of this paper is the extension of the state-of-the-art, i.e., deterministic AC SCOPF, to capture jointly two new dimensions (RES stochasticity and multiple time periods) as well as the emerging sources of flexibility (FL and ESS)*. In other words, the paper proposes and solves for the first time a new problem formulation in the form of a stochastic multi-period AC SCOPF (S-MP-SCOPF).

A direct approach relying on the state-of-the-art NLP solver IPOPT [36], widely used in many AC OPF/SCOPF applications, is conducted tackling the largest problem size that the solver can still manage while a tractable solution algorithm is planned for future work. Note that the challenging size of the proposed S-MP-SCOPF problem is determined by the product of four different dimensions: the size of the system, number of postulated contingencies, number of uncertainty scenarios and number of time periods.

To further highlight the above mentioned novel contributions of this work, Table 1 summarizes the main modelling features of the proposed approach which distinguishes it from the several existing methods. One can observe that, like this work, scalability is not pursued per se in most works that address more challenging AS SCOPF problem extensions. Also, it is implied that if AC grid model is not used, then simplified models (e.g. DC) are adopted.

The remaining of the paper is organized as follows. Section 2 presents the detailed formulation of the S-MP-SCOPF problem. Section 3 provides quantitative results with a direct approach to the proposed problem. Section 4 concludes and provide directions for future works.

2. Formulation of the S-MP-SCOPF problem

This section describes in detail the proposed S-MP-SCOPF model to procure, in day-ahead operation planning, flexibility for congestion management and voltage control such that to satisfy N-1 security criterion. The model computes optimal set-points for flexibility resources (FL and ESS), RES curtailment and other conventional control means (e.g., generators) in each time period and system state. As illustrated in Fig. 1, normalized scenario profiles over 24-hour period which are generated using a time series based Auto regressive integrated moving average (ARIMA) [37] model along with network topology data, set of $N-1$ contingencies, and cleared generators' active power in energy market are inputs of the proposed model. Note that any other scenario generation method such as Monte Carlo simulation accompanied with any scenario reduction/ clustering technique such as k-means, [38], can be plugged into the proposed model.

The model relies on AC power flow equations using voltages expressed in rectangular coordinates.

A modelling aspect worth discussing for any stochastic optimization problem is the number of decision-making stages assumed. In day-ahead operation planning, there may be two such stages corresponding to "here and now" (H&N) or scenario-independent decisions and "wait and see" (W&S) or scenario-dependent decisions stages. H&N decision variables in our problem refer to large size slow generators, whose generation scheduling is independent of RES scenario realizations, while W&S decision variables refer to fast response generators that can be redispatched depending upon RES scenario realization. Choosing the adequate combination of these two decisions is context-dependent, i.e. it depends on the operator preference as well as type of available generators. For example, in a system with high percentage of slow responding nuclear power plants, one would favour H&N decisions while in future power systems targeted in this work, dominated by variable RES (even with 100% RES penetration), one would favour only W&S decisions. Accordingly, in what follows, we will formulate first the S-MP-SCOPF problem with only single stage W&S decisions which we advocate in this work and use unless mentioned otherwise. Later, we will extend the problem formulation to two decision-making stages including both H&N and W&S decisions. Numerical results will be provided with both these decision making options.

2.1. Single-stage S-MP-SCOPF model based on W&S decision variables

The single-stage S-MP-SCOPF problem formulation is presented in (1)–(23). The objective (1) is to minimize the expected cost of flexibility procurement for ancillary services (congestion and voltage control) in transmission network operation under both normal (pre-contingency) and post contingency states. This cost pertains to the re-dispatch of conventional generators, ESS, FL, curtailment of RES and load curtailment to prevent infeasibility.

$$\min \sum_{s\in S}\sum_{t\in T}\pi_s\Bigg\{\sum_{g\in G}\left|P^0_{G_{g,s,t}} - P^*_{G_{g,t}}\right| c_g$$

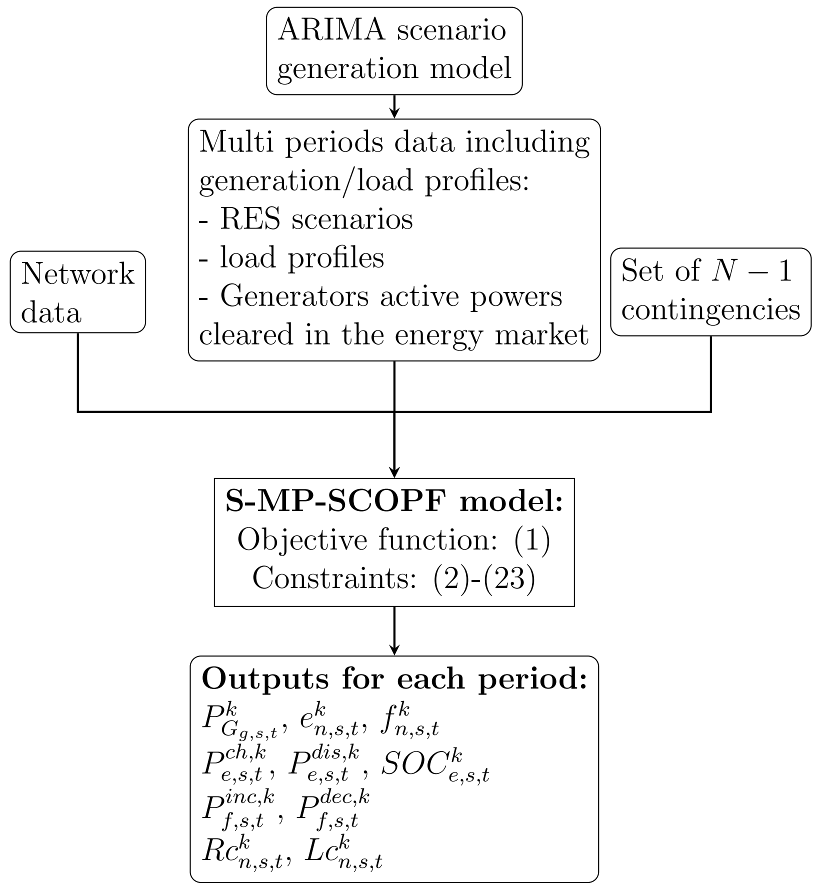

Fig. 1. Flowchart of the proposed model.

$$
\begin{aligned}
&+ \sum_{k\in K}\Bigg[\sum_{e\in E}\left(P^{ch,k}_{e,s,t}+P^{dis,k}_{e,s,t}\right)c_e \\
&+ \sum_{f\in F}\left(P^{inc,k}_{f,s,t}+P^{dec,k}_{f,s,t}\right)c_f \\
&+ \sum_{n\in R}\left(Rc^k_{n,s,t}\right)c^{Gcurt}_n+\sum_{n\in N}\left(Lc^k_{n,s,t}\right)c^{Lcurt}_n\Bigg]\Bigg\}
\end{aligned}
\tag{1}
$$

The problem is subject to the following constraints:

$$
\begin{aligned}
&\sum_{g\in G}P^k_{G_{g,s,t}}+R_{n,s,t}+\sum_{e\in E}\left(P^{dis,k}_{e,s,t}-P^{ch,k}_{e,s,t}\right) \\
&+\sum_{f\in F}\left(P^{dec,k}_{f,s,t}-P^{inc,k}_{f,s,t}\right)-Rc^k_{n,s,t}+Lc^k_{n,s,t}= \\
&P_{D_{n,t}}+P^k_{inj_{n,s,t}} \\
&\forall n\in N, s\in S, t\in T, k\in K
\end{aligned}
\tag{2}
$$

$$
\begin{aligned}
&\sum_{g\in G}Q^k_{G_{g,s,t}}=Q_{D_{n,t}}-Q_{c_{n,s,t}}+Q^k_{inj_{n,s,t}} \\
&\forall n\in N, s\in S, t\in T, k\in K
\end{aligned}
\tag{3}
$$

$$
\begin{aligned}
&P^k_{inj_{n,s,t}}=\left[\left(e^k_{n,s,t}\right)^2+\left(f^k_{n,s,t}\right)^2\right]\sum_{m\in N}G_{nm} \\
&-\sum_{m\in N}[\left(e^k_{n,s,t}e^k_{m,s,t}+f^k_{n,s,t}f^k_{m,s,t}\right)G_{nm} \\
&+\left(f^k_{n,s,t}e^k_{m,s,t}-e^k_{n,s,t}f^k_{m,s,t}\right)B_{nm}] \\
&\forall n\in N, s\in S, t\in T, k\in K
\end{aligned}
\tag{4}
$$

$$
\begin{aligned}
&Q^k_{inj_{n,s,t}}=-\left[\left(e^k_{n,s,t}\right)^2+\left(f^k_{n,s,t}\right)^2\right]\sum_{m\in N}\left(B^{sh}_{nm}+B_{nm}\right) \\
&+\sum_{m\in N}[\left(e^k_{n,s,t}e^k_{m,s,t}+f^k_{n,s,t}f^k_{m,s,t}\right)B_{nm} \\
&-\left(f^k_{n,s,t}e^k_{m,s,t}-e^k_{n,s,t}f^k_{m,s,t}\right)G_{nm}] \\
&\forall n\in N, s\in S, t\in T, k\in K
\end{aligned}
\tag{5}
$$

$$
\underline{P}_g\le P^k_{G_{g,s,t}}\le\overline{P}_g \qquad \forall g\in G, s\in S, t\in T, k\in K
\tag{6}
$$

$$
\underline{Q}_g\le Q^k_{G_{g,s,t}}\le\overline{Q}_g \qquad \forall g\in G, s\in S, t\in T, k\in K
\tag{7}
$$

$$
\begin{aligned}
&\left(G^2_{nm}+B^2_{nm}\right)\left[\left(e^k_{n,s,t}-e^k_{m,s,t}\right)^2+\left(f^k_{n,s,t}-f^k_{m,s,t}\right)^2\right] \\
&\le\left(I^{\max}_{nm}\right)^2 \qquad \forall n,m\in N, s\in S, t\in T, k\in K
\end{aligned}
\tag{8}
$$

$$
\begin{aligned}
&\left(\underline{V}_n\right)^2\le\left(e^k_{n,s,t}\right)^2+\left(f^k_{n,s,t}\right)^2\le\left(\overline{V}_n\right)^2 \\
&\qquad\forall n\in N, s\in S, t\in T, k\in K
\end{aligned}
\tag{9}
$$

$$
\left|P^0_{G_{g,s,t-1}}-P^0_{G_{g,s,t}}\right|\le\Delta P_{G_g} \quad \forall g\in G, s\in S, t\in T
\tag{10}
$$

$$
\begin{aligned}
&\left|P^k_{G_{g,s,t}}-P^0_{G_{g,s,t}}\right|\le\Delta P_{G_g} \\
&\qquad\forall g\in G, s\in S, t\in T, k\in K, k\ne 0
\end{aligned}
\tag{11}
$$

$$
\begin{aligned}
&SOC^k_{e,s,t+1}=SOC^k_{e,s,t}+\Delta T\left(\eta^{ch,e}P^{ch,k}_{e,s,t}-P^{dis,k}_{e,s,t}/\eta^{dis,e}\right) \\
&\forall e\in E, s\in S, t\in T, k\in K
\end{aligned}
\tag{12}
$$

$$
\begin{aligned}
&SOC^{min}_e\le SOC^k_{e,s,t}\le SOC^{max}_e \\
&\forall e\in E, s\in S, t\in T, k\in K
\end{aligned}
\tag{13}
$$

$$
SOC^k_{e,s,T}=SOC^k_{e,s,0}, \forall e\in E, s\in S, t\in T, k\in K
\tag{14}
$$

$$
0\le P^{ch,k}_{e,s,t}\le\overline{P}^{ch}_e, \forall e\in E, s\in S, t\in T, k\in K
\tag{15}
$$

$$0 \le P^{dis,k}_{e,s,t} \le \overline{P}^{dis}_{e}, \forall e \in E, s \in S, t \in T, k \in K \tag{16}$$

$$\frac{P^{ch,k}_{e,s,t}}{\overline{P}^{ch}_{e}} + \frac{P^{dis,k}_{e,s,t}}{\overline{P}^{dis}_{e}} \le 1, \forall e \in E, s \in S, t \in T, k \in K \tag{17}$$

$$\sum_{t \in T} P^{inc,k}_{f,s,t} = \sum_{t \in T} P^{dec,k}_{f,s,t}, \forall f \in F, s \in S, t \in T, k \in K \tag{18}$$

$$0 \le P^{inc,k}_{f,s,t} \le \overline{P}^{inc}_{f}, \forall f \in F, s \in S, t \in T, k \in K \tag{19}$$

$$0 \le P^{dec,k}_{f,s,t} \le \overline{P}^{dec}_{f}, \forall f \in F, s \in S, t \in T, k \in K \tag{20}$$

$$\frac{P^{dec,k}_{f,s,t}}{\overline{P}^{dec}_{f}} + \frac{P^{inc,k}_{f,s,t}}{\overline{P}^{inc}_{f}} \le 1, \forall f \in F, s \in S, t \in T, k \in K \tag{21}$$

$$0 \le Lc^{k}_{n,s,t} \le P_{D_{n,t}}, \forall n \in N, s \in S, t \in T, k \in K \tag{22}$$

$$0 \le Rc^{k}_{n,s,t} \le R_{n,s,t}, \forall n \in N, s \in S, t \in T, k \in K \tag{23}$$

where $k = 0$ represents normal operation state while $k \ge 1$ indicates contingency states, all notations being defined in the nomenclature.

Constraints (2) and (3) represent active and reactive power balance equations (for each node n, scenario s, time t and state k), which include active/reactive power flows from (4) and (5). Note that in (3) load curtailment assumes constant power factor.

Constraints (6) and (7) are the hard physical limits on active and reactive powers of generator g.

Network operation constraints (congestion and voltages) are modelled by constraints (8) and (9). Eq. (8) represents the longitudinal branch current limit, which is a reasonable approximation of the current aimed to avoid doubling the number of constraints (e.g., when the current is expressed for both ends of the branch). Eq. (9) imposes limits on node voltage magnitude.

Eq. (10) restricts the ramping of generator g for each two successive time intervals of normal operating state. Eq. (11) is the coupling constraint on active power of generator g between normal operation and post-contingency states.

The ESS operation is captured by the following set of constraints [39]. Eq. (12) describes the dynamics of State-of-Charge (SoC), (13) is the SoC limit for each ESS, (14) maintains the SoC of ESS equal on first and last time periods, (15) and (16) are limits on active power charging and discharging of ESS and (17) prevents the simultaneous charging and discharging of storage e for each period.

It is important to note that (17) is a smart and tractable exact approximation, proposed in [40] to avoid introducing binary variables to model the statuses charging and discharging of an ESS. In the latter work it is demonstrated that this modelling approach imitates exactly the behaviour of binary variables, i.e., at the optimum, an ESS either charges or discharges but not both. This is due to the fact that both charging and discharging status have associated costs in the objective function which in turn prevents the simultaneous charging and discharging of an ESS. This effect is also empirically observed in all our numerical simulations.

The FL operation is modelled by the following set of constraints. Eq. (18) maintains the energy balance of a FL over whole time horizon, (19) and (20) are the limits on the increase and decrease of active power of FL, respectively, and (21) prevents simultaneous increase and decrease in the active power of FL during each time interval. Remark that (21) relies on the same type of assumption and approximation as for storage elements in (17).

Finally, (22) limits the load curtailment while (23) restricts the RES curtailment.

Note that the proposed S-MP-SCOPF is an NLP problem. Finally, when only W&S decisions are considered, the single stage S-MP-SCOPF problem can be decomposed per scenario in a series of deterministic multiperiod SCOPF (D-MP-SCOPF), as shown in Fig. 2, and if parallel computations are implemented, computation efficiency can be greatly improved.

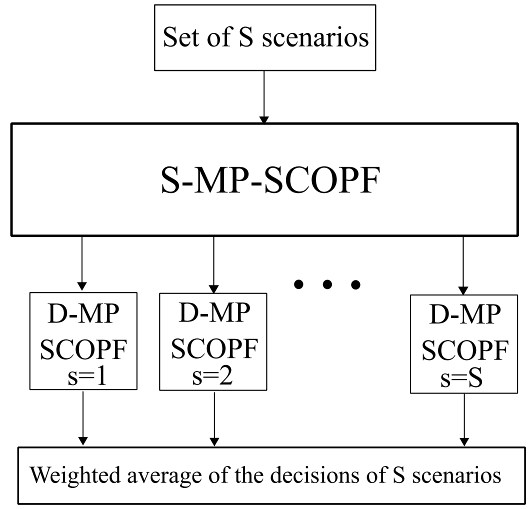

Fig. 2. Decomposition of the proposed S-MP-SCOPF into a series of D-MP-SCOPF to take advantage from parallel computation.

The proposed model relates with energy and ancillary service markets in the following way. It is assumed that first energy market is cleared without (considering accurate models for) power flow constraints. Then the TSO runs the proposed grid operation model taking into account the active power set points of the conventional generators, cleared in the market, to guarantee feasible operation conditions. As the market may not lead to a generation dispatch that satisfies all constraints, the TSO may have to re-dispatch some generators (together with other control means) at minimum re-dispatch cost. Specific markets may also clear additional reserves (e.g. for frequency control) before this SCOPF is run which are not in the scope of this paper. Indeed in SCOPF frameworks operating reserves such as spinning reserve are typically not considered. Our SCOPF handles only static constraints (voltages and currents). However, if available from some ancillary services market clearing, the presence of additional reserves may be modelled in our SCOPF problem, as similarly done in [41]. In such a case, our SCOPF may lead to procure further reserves, in top of those already cleared in the market, to satisfy N-1 security with respect to static constraints.

2.2. Two-stage S-MP-SCOPF model based on H&N and W&S decision variables

In this subsection, we briefly explain the two-stage S-MP-SCOPF problem formulation by considering both H&N and W&S decisions. To this end, the set of generators G is divided into two subsets, namely scenario independent H&N generators (G_h) and scenario dependent W&S generators (G_w). This leads to the following changes in the single-stage S-MP-AC SCOPF model presented in the previous section.

- The objective function (1) becomes:

$$\min \sum_{t \in T} \sum_{g \in G_h} \left| P^{0}_{G_{g,t}} - P^{*}_{G_{g,t}} \right| c_g$$

$$+ \sum_{t \in T} \sum_{s \in S} \pi_s \sum_{g \in G_w} \left\{ \left(P^{0}_{G_{g,s,t}} - P^{*}_{G_{g,t}} \right) c_g \right.$$

$$+ \sum_{k \in K} \left[\sum_{e \in E} \left(P^{ch,k}_{e,s,t} + P^{dis,k}_{e,s,t} \right) c_e \right.$$

$$+ \sum_{f \in F} \left(P^{inc,k}_{f,s,t} + P^{dec,k}_{f,s,t} \right) c_f$$

$$+\sum_{n\in R}\left(Rc^{k}_{n,s,t}\right)c^{Gcurt}_{n}+\sum_{n\in N}\left(Lc^{k}_{n,s,t}\right)c^{Lcurt}_{n}\Bigg]\Bigg\} \tag{24}$$

- Eq. (2) is replaced with two following equations:

$$\sum_{g\in G_h}P^0_{G_{g,t}}+\sum_{g\in G_w}P^k_{G_{g,s,t}}+R_{n,s,t}$$
$$+\sum_{e\in E}\left(P^{dis,k}_{e,s,t}-P^{ch,k}_{e,s,t}\right)+\sum_{f\in F}\left(P^{dec,k}_{f,s,t}-P^{inc,k}_{f,s,t}\right)$$
$$-Rc^k_{n,s,t}+Lc^k_{n,s,t}=P_{D_{n,t}}+P^k_{inj_{n,s,t}}$$
$$\forall n\in N,s\in S,t\in T,k\in K,k\neq 0 \tag{25}$$

$$\sum_{g\in G_h}P^0_{G_{g,t}}+\sum_{g\in G_w}P^0_{G_{g,s,t}}+R_{n,s,t}$$
$$+\sum_{e\in E}\left(P^{dis,0}_{e,s,t}-P^{ch,0}_{e,s,t}\right)+\sum_{f\in F}\left(P^{dec,0}_{f,s,t}-P^{inc,0}_{f,s,t}\right)$$
$$-Rc^0_{n,s,t}+Lc^0_{n,s,t}=P_{D_{n,t}}+P^0_{inj_{n,s,t}}$$
$$\forall n\in N,s\in S,t\in T \tag{26}$$

- Eqs. (10) and (11) are replaced with the following coupling constraints, respectively:

$$\left|P^k_{G_{i,s,t}}-P^0_{G_{i,s,t}}\right|\le \Delta P_{G_i}$$
$$\forall i\in G_w,s\in S,t\in T,k\in K,k\neq 0 \tag{27}$$

$$\left|P^0_{G_{i,s,t-1}}-P^0_{G_{i,s,t}}\right|\le \Delta P_{G_i}\quad \forall i\in G_w,s\in S,t\in T \tag{28}$$

$$\left|P^0_{G_{i,t-1}}-P^0_{G_{i,t}}\right|\le \Delta P_{G_i}\quad \forall i\in G_h,t\in T \tag{29}$$

Clearly, the utilization of H&N decisions reduces the size of S-MP-SCOPF problem. The size reduction stems from the fact that the number of decision variables regarding active and reactive power outputs of large slow generators will be reduced by assuming them to be independent of RES scenarios. However, the problem cannot be decomposed straightforwardly as for only W&S decisions, see Fig. 2.

Last but not least, a practical aspect of any stochastic optimization problem is the interpretation/implementation of the optimal stochastic solution of W&S variables, see Fig. 1. If only W&S decisions are used, the obtained stochastic solution can be averaged and implemented by the operator as H&N decisions. Weighted or aggregated W&S decisions, however, do not guarantee to satisfy all constraints but produce at least a picture of the next day possible scenarios. Nevertheless, the TSO can still choose the specific settings of one likely scenario, which are by default feasible once the SCOPF problem is feasible. As regards the combination of W&S and H&N decisions, they can clearly be employed by the power system operators practically as their feasibility is guaranteed.

3. Numerical results

The features of the proposed S-MP-SCOPF model are illustrated using two test systems of 5 and 60 nodes respectively, for 24-hours time frame (one hour time resolution), given sets of N-1 contingencies and different number of scenarios.

We focus on solving the S-MP-SCOPF problem with only single stage W&S decisions unless mentioned otherwise. All simulations are performed in Julia/JuMP open source programming language [42] on a PC of 2.11 GHz and 48 GB of RAM. IPOPT optimizer is used to solve all NLP problems [36]. In all simulations, the base apparent power is set to 100 MVA.

3.1. Results for 5-node test system

The 5 node system is adopted from [6] and its one-line diagram is shown in Fig. 3. We consider 6 N-1 line contingencies and up to 10 uncertainty scenarios. Full results for this test case are comprehensively

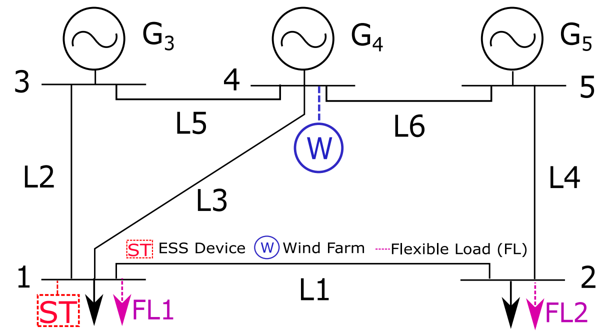

Fig. 3. One-line diagram of the 5-bus system.

discussed and all necessary data are provided to enable benchmarking, reproducibility and comparison (see Tables 2 and 3).

To consider RES, a wind farm is deployed at node 4. Fig. 4 shows ten normalized scenario profiles over 24-hour period which are generated using a time series based ARIMA model. The scenarios and contingencies are equiprobable and (for simplicity) loads are assumed constant for the entire 24 h horizon. For the sake of illustrative purposes, we neglected loads uncertainty as, in day-ahead, this is generally much lower than the uncertainty related to wind power production. In other words, forecasting error of loads in transmission network are deemed acceptable for operators as opposite to wind power production. However, the proposed model can include loads uncertainty straightforwardly in the same manner as wind power uncertainty. Four case studies are developed to assess the capability of the proposed model (in all cases load and RES generation curtailment is allowed to prevent infeasible problems):

- Case#0: no FL or ESS are considered;
- Case#1: one ESS is embedded at node 1 with the parameters provided in Table 4 and c_e cost is set to 80 €/MWh;
- Case#2: 10% of load at node 1 and 2 (FL1 and FL2 in Fig. 3) is assumed flexible and the c_f cost is set to 80 and 40 €/MWh, respectively in all operation states;
- Case#3: both ESS and FL are allowed to take part in optimization, with the costs given above.

3.1.1. Case#0

Table 5 compares the results of the proposed model for different RES capacities, where RC0-RC10, CG and LC stand for RES capacity (between 0 and 1000 MW), conventional generation and load curtailment, respectively. It can be observed that as the penetration rate of RES increases, CG cost reduces gradually since the RES production is paid by feed-in-tariff. However, the cost of curtailed energy increases up to 105,294 € in RC10. This suggests that efficient utilization of flexibility resources can potentially reduce the amount of curtailed energy.

3.1.2. Case#1

Table 6 provides the proposed model results with ESS at node 1 for different RES capacities. In comparison with the base case (i.e. Case#0) the curtailment cost is reduced up to 46% (i.e., $(105,294-56,754)/105,294$€) and the total cost reduces by $1,631,997-1,595,907=$ 36,090€ for RC10. In addition, the flexibility added by ESS prevents load curtailment in case RC7.

3.1.3. Case#2

Similar benefits are observed using FL in both nodes 1 and 2 as shown in Table 7. Using the flexibility provided by FL causes no energy curtailment for RC7 and RC8. Even in the case RC10, the total curtailment cost is reduced to 62% (i.e., $(105,294-40,001)/105,294$€). In addition, the total cost for RC10 is reduced by 2.75% with respect to the base case.

Table 2
5-bus system data at peak load with no wind, no storage and no flexible load.

bus	P_L MW	Q_L MVar	P_G MW	Q_G MVar	V pu	V^{min} pu	V^{max} pu	P_G^{min} MW	P_G^{max} MW	Q_G^{min} MVar	Q_G^{max} MVar	ΔP_G MW	a €/MWh^2	b €/MWh	c €
1	1100	400	–	–	0.954	0.92	1.05	–	–	–	–	–	–	–	–
2	500	200	–	–	0.950	0.92	1.05	–	–	–	–	–	–	–	–
3	–	–	700.0	69.5	1.0	0.92	1.05	150	1500	−500	750	200	0.01	25	100
4	–	–	600.0	304.9	1.0	0.92	1.05	150	1500	−500	750	200	0.01	60	100
5	–	–	333.8	146.9	1.0	0.92	1.05	150	1500	−500	750	200	0.01	30	100

a, b, c: Cost coefficients of conventional generators in nonlinear form $aP_G^2 + bP_G + c$.

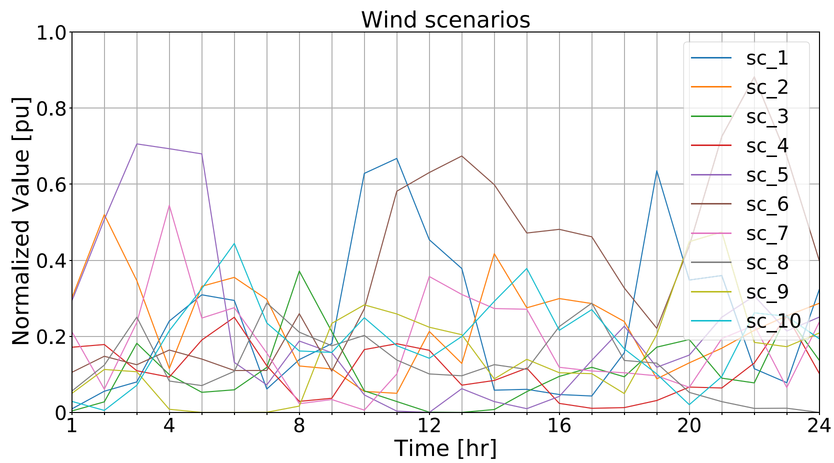

Fig. 4. Wind power scenarios profile (normalized values).

Table 3
5-bus system: line data.

Line	bus n	bus m	V^{nom} kV	R_{nm} Ω	X_{nm} Ω	B_{nm} μS	I_{nm}^{max} A
L1	1	2	400	3.2	16	160	1587.7
L2	1	3	400	6.4	32	320	1587.7
L3	1	4	400	3.2	16	160	1587.7
L4	2	5	400	6.4	32	320	1587.7
L5	3	4	400	6.4	32	320	1587.7
L6	4	5	400	6.4	32	320	1587.7

Table 4
ESS characteristics.

bus	SOC_e^{min} MWh	SOC_e^{max} MWh	$\overline{P}_e^{ch}$ MW	$\overline{P}_e^{dis}$ MW	$\eta^{ch,e}$	$\eta^{dis,e}$
1	660	2200	50	50	0.95	0.95

3.1.4. Case#3

The results for the proposed S-MP-SCOPF model considering both ESS and FL are summarized in Table 8. It can be seen that no energy curtailment occurs for RC7 and RC9. In addition, the curtailment cost decreases by 90.5% (i.e. $(105,294 - 10,001)/105,294$€). This suggests that efficient utilization of flexibility resources can potentially reduce the amount of curtailed energy. One can also observe that the total cost is reduced by 4% with respect to the base case.

Another important remark is the synergy benefit of using FL and ESS flexibility sources simultaneously as can be noticed by the reduced cost of FL (9.88%) and ESS (27.2%) in comparison to the results reported for the Case#1 and Case#2 in Tables 6 and 7, respectively.

The computation time of the NLP problem is short in the range of few tens of seconds. Despite the small system size (5 nodes), the corresponding S-MP-SCOPF problem includes 7 operation states, 24 time periods and 10 scenarios which corresponds to roughly equivalent in size of solving an AC OPF problem for a system of around 8,400[1] nodes.

For all case studies, the only binding contingency is the disconnection of line L2. For this contingency, in Case#3 and RC10, Fig. 5 illustrates the state of charge (SoC) profile for scenario 8 (i.e., s8 in Fig. 4) while Fig. 6 plots the ESS and FL profiles. As expected, to accommodate maximum wind power in the network, ESS discharges in periods with excess wind (i.e., 7–14) while FL decreases the load (i.e., underdemand) during the same time-periods. To maintain their daily energy balance equal to zero, both ESS and FL increase charging and load to hours of low wind generation (i.e., 1–6 and 16–24).

Fig. 7 illustrates the load curtailment for scenario s8 and contingency in line L2. A decreasing trend can be observed from Case#0 to Case#3 by considering the flexibility of ESS and FL. For instance, at 12 pm, the curtailed power reduces by 72% (i.e., $(1.714-0.42)/1.714$) when considering both ESS and FL. This further demonstrates the benefits of additional flexibility offered by ESS and FL.

3.2. Results for Nordic32 test system

To test model scalability, we use the synthetic Nordic32 test system [43], which is closely inspired by the Sweden system. The test system includes 60 nodes, 23 generators, 57 lines, 31 transformers, and 12 shunts reactors/capacitors [43]. A contingency set of 33 N-1 line disconnections is assumed. We assume a futuristic renewable-dominated version of this system (see Fig. 8), in which five large wind farms (with 7200, 5400, 6300, 5700, and 6300 MW of rated power) are installed at nodes 1012, 1013, 1014, 4021 and 4042, respectively. The penetration rate of wind generation as compared to the total generation capacity is 18.84% (i.e. $100 * (163,950\text{ MW} - 30,900\text{ MW})/163,950\text{ MW}$). However, overall Sweden's generation capacity and electricity production roughly comes from dispatchabe renewable hydroelectric (45%)

[1] operation states (7) × time periods (24) × scenarios (10) × nodes (5).

Table 5
Case#0 SCOPF results for different RES capacities.

RES cases	RES (MW)	CG cost (€)	LC cost (€)	Total cost (€)	Time (s)
RC0	0	1,693,208	0	1,693,208	12
RC1	100	1,676,410	0	1,676,410	11
RC2	200	1,659,782	0	1,659,782	12
RC3	300	1,643,324	0	1,643,324	11
RC4	400	1,627,036	0	1,627,036	12
RC5	500	1,610,917	0	1,610,917	13
RC6	600	1,594,967	0	1,594,967	14
RC7	700	1,578,949	2,287	1,581,236	21
RC8	800	1,560,524	2,8060	1,588,584	25
RC9	900	1,543,530	57,444	1,600,974	25
RC10	1,000	1,526,703	105,294	1,631,997	26

CG: Conventional Generation.
LC: Load Curtailment.

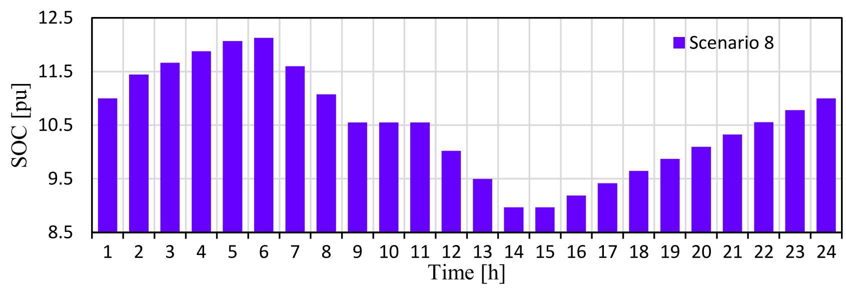

Fig. 5. SOC profile of ESS for scenario 8 in contingency in line L2.

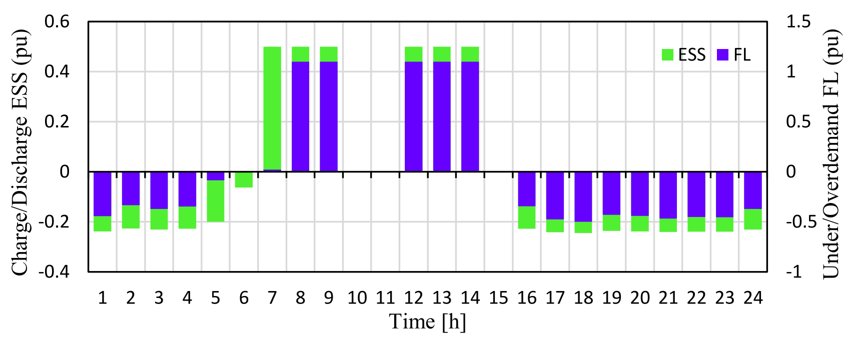

Fig. 6. Injection and absorption profile of active power for both ESS and FL in contingency in line L2.

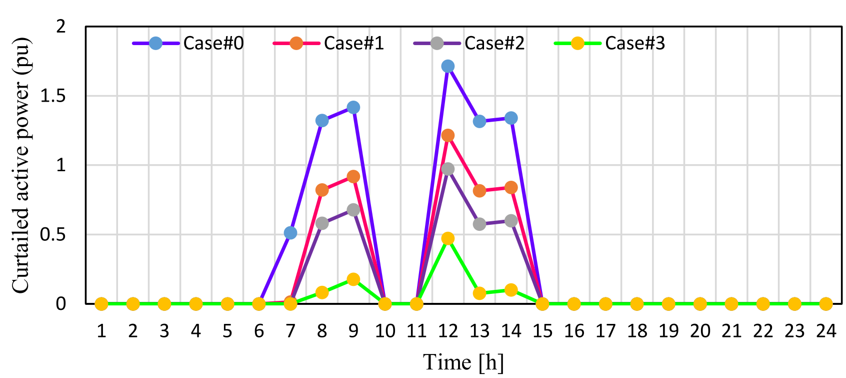

Fig. 7. Curtailed active power profile for four cases: contingency L2 and s8.

and low-carbon nuclear (30%) power, [43]. As such, renewable generation, dispatchable and variable, dominates the electricity mix. As a consequence, to cope with the uncertain variability and potential excess of active power injected in north area while managing congestion and voltage issues, three FL are assumed at nodes 1011, 1044, and 2031, and two ESS (with the same parameters as in Table 4) are embedded at nodes 1045 and 4046. The load pattern from [44] is adopted for a generic summer day. To test the scalability of the proposed model, we consider up to 30 scenarios.

3.2.1. *Illustration of flexibility resources*

In this subsection, the performance of the emerging flexibility resources on the Nordic32 test system is evaluated. To evaluate the added value of using emerging flexible resources (FL and ESS), like

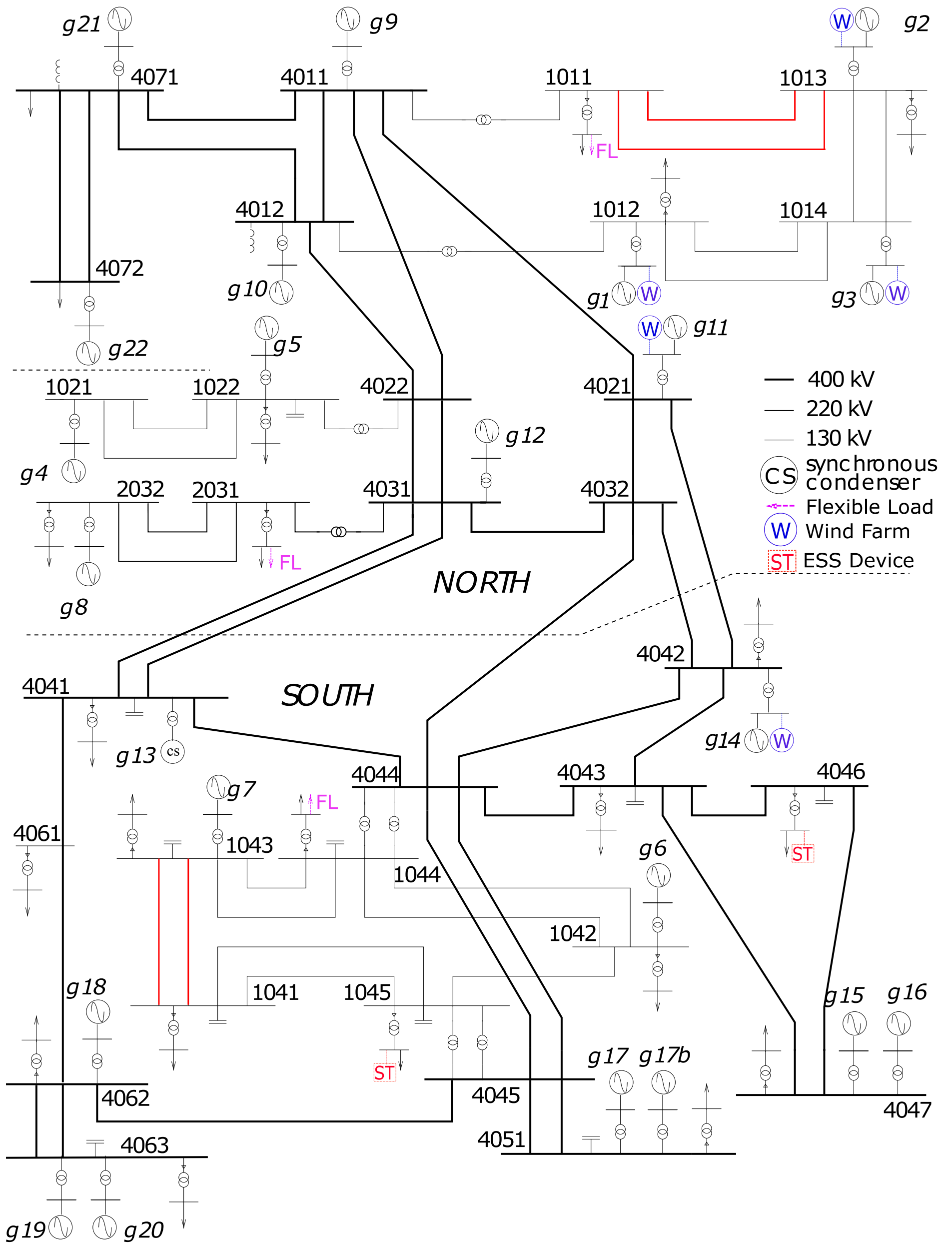

Fig. 8. One-line diagram of Nordic32 test system.

Table 6
Case#1 SCOPF results with ESS for different RES capacities.

RES cases	CG cost (€)	LC cost (€)	ESS cost (€)	Total cost (€)	Time (s)
RC0	1,693,208	0	0	1,693,208	12
RC1	1,676,410	0	0	1,676,410	13
RC2	1,659,782	0	0	1,659,782	13
RC3	1,643,324	0	0	1,643,324	13
RC4	1,627,036	0	0	1,627,036	13
RC5	1,610,917	0	0	1,610,917	14
RC6	1,594,967	0	0	1,594,967	16
RC7	1,579,193	0	389	1,579,582	23
RC8	1,563,451	2,064	4,390	1,569,905	27
RC9	1,546,819	26,052	5,300	1,578,171	32
RC10	1,530,821	56,754	8,332	1,595,907	27

Table 7
Case#2 SCOPF results with FL for different RES capacities.

RES cases	CG Cost (€)	LC cost (€)	FL cost (€)	Total cost (€)	Time (s)
RC0	1,693,208	0	0	1,693,208	12
RC1	1,676,410	0	0	1,676,410	13
RC2	1,659,782	0	0	1,659,782	13
RC3	1,643,324	0	0	1,643,324	13
RC4	1,627,036	0	0	1,627,036	13
RC5	1,610,917	0	0	1,610,917	13
RC6	1,594,967	0	0	1,594,967	14
RC7	1,579,165	0	550	1,579,715	26
RC8	1,563,507	0	6,710	1,570,217	20
RC9	1,548,656	11,780	10,899	1,571,335	29
RC10	1,532,739	40,001	14,377	1,587,117	33

for the 5-bus system, four different case studies are defined, namely: Case#0 (base case) in which neither FL nor ESS are used, Case#1 where only ESS units are utilized, Case#2 where only FL are considered, and finally, Case#3 where both ESS and FL units are available. For all cases, 10 wind scenarios are generated, the ESS cost is set to 3 €/MWh

Table 8
Case#3 SCOPF results with ESS and FL for 10 RES capacities.

RES cases	CG cost (€)	LC cost (€)	FL cost (€)	ESS cost (€)	Total cost (€)	Time (s)
RC0	1,693,208	0	0	0	1,693,208	14
RC1	1,676,410	0	0	0	1,676,410	14
RC2	1,659,782	0	0	0	1,659,782	14
RC3	1,643,324	0	0	0	1,643,324	14
RC4	1,627,036	0	0	0	1,627,036	14
RC5	1,610,917	0	0	0	1,610,917	14
RC6	1,594,967	0	0	0	1,594,967	15
RC7	1,579,193	0	0	389	1,579,582	26
RC8	1,563,707	0	491	4,390	1,568,588	24
RC9	1,550,080	0	6200	5,299	1,561,579	23
RC10	1,536,615	10,001	12,956	6,065	1,565,637	30

Table 9
Nordic32 test system results for different case studies.

Cases	Normal operation state					Post contingency state				Total cost (€)
	CG cost (€)	LC cost (€)	GC cost (€)	FL cost (€)	ESS cost (€)	LC cost (€)	GC cost (€)	FL cost (€)	ESS cost (€)	
Case#0	212,184	0.0	16,726	–	–	1,791	26,754	–	–	257,456
Case#1	211,688	0.0	16,726	–	0.0	1,791	26,758	–	382	257,344
Case#2	212,161	0.0	16,153	226	–	1,791	25,873	364	–	256,571
Case#3	211,675	0.0	16,158	226	0.0	1,791	25,880	361	369	256,464

and FL cost is set to 2.5€/MWh for both normal operation and post-contingency states. The load and generation curtailment cost is set to 30€/MWh i.e., ten times larger than the most expensive conventional generator cost.

Table 9 provides the different components of the total expected cost for the different cases. In Case#0, the total cost equals 257,456€ and wind generation curtailment occurs in both normal and post contingency states. However, thanks to the additional flexibility offered by the ESS in node 1045, the conventional operation cost reduces from 212,184€ in the Case#0 to 211,688€ in the Case#1. As a result, although an additional cost regarding the activation of ESS is imposed in the post contingency state, total cost decreases from 257,456€ to 257,344€. In Case#2, although the conventional generators' cost remains almost constant, the wind generation curtailment cost is reduced significantly from 26,754€ in the base case to 25,873€ in Case#2. Consequently, the total expected cost reduces by 885€ (i.e. $257,456 - 256,571 = 885$€) as compared to the base case. In addition, in Case#2, the wind power curtailment cost in normal operation is also reduced by 573€ (i.e. $16,726 - 16,153 = 573$€). The same trend can be observed in the last case, Case#4, where both ESS and FL are activated in the post contingency state, where the additional volume of flexibility causes a total expected cost reduction of 992€ (i.e., from 257,456€ in Case#0 to 256,464€ in Case#3).

These results demonstrate that flexible resources (ESS and FL) can contribute cost-effectively to a reduction of wind energy spillage and load curtailment, improving the overall system flexibility, and allowing thereby to accommodate larger amounts of renewables.

Figs. 9, 10, and 11 illustrate the flexible resources behaviour at the solution of the proposed S-MP-SCOPF model. Fig. 9 shows the SoC profile of ESS at node 1045 in scenario s1 and the contingency in a single line circuit between nodes 1041 and 1043, which overloads the second line circuit in parallel between the same nodes, both coloured in red in Fig. 8. As expected, to alleviate the overload in the second circuit of line 1041–1043 in periods with high demand, ESS discharges during peak hours (i.e., 17–20) and charges during the lower demand hours where the line is less loaded to maintain its energy balance constraint (see Fig. 9).

The FL at node 1011 in the same scenario and contingency shows apparently a counter-intuitive behaviour. As can be seen in Fig. 10, FL decreases the load during hours with extra wind power generation and, to maintain its daily energy balance, increases the load in hours with high load. This behaviour can be justified as follows. In hours 7–9 and 12–14, when wind farms generate large amount of wind power, the lines between nodes 1011 and 1013, shown with red colour in Fig. 8, are congested in both normal and post-contingency states. These bottlenecks require the activation of FL to remove these congestions (by creating counter-flows) and minimize the wind power curtailment. In conclusion, the primary functionality of FL is driven by the prevention of current/voltage constraints violation rather than the simpler power balance satisfaction needs.

Fig. 11 shows voltage profile for bus 1045 for two cases, namely with and without ESS and contingency in connecting line 1041 and 1043 under scenario sc_8. Compared to Fig. 10, when ESS charges during the lower demand hours the voltage magnitude is decreased while during peak hours voltage magnitude is mostly equal or increased slightly due to the discharging of ESS.

3.2.2. Model scalability

In this subsection, the scalability test is performed for the proposed model against increasing number of scenarios and thereby the problem size. Table 10 shows the results of the scalability test of the proposed S-MP-SCOPF model for increasing number of scenarios. The results are obtained with IPOPT solver using default setting except of the relative optimality gap tolerance, which is set to 10^{-5}.

Note that while increasing the problem size, the elapsed time grows sharply with non-monotonic slope. For instance, although the problem size increases ten times from 1 scenario to 10 scenarios, the computation time increases more than 19.7 times (i.e., $(5,985 - 289)/289$). In addition, the largest number of scenarios the solver can handle reliably is 30, which corresponds to a huge NLP optimization problem with roughly 5 millions continues variables and 9 millions of constraints, which is solved in 22,110 s. For larger number of scenarios, the default linear (system of equations) solver package MUMPS in IPOPT fails to allocate memory even before IPOPT can start iterations. An interesting observation regarding IPOPT solver is that, as for other interior-point method-based solvers, the iteration number is little dependent on the size of the problem.

Note that the computation time can be further significantly improved by using another linear solver in IPOPT. For example, it is reported at https://github.com/power-grid-lib/pglib-opf/blob/master/BASELINE.md that ma27 linear solver can decrease the runtime by 2–6 times as compared to default linear solver MUMPS. However, we did not manage to compile and plug ma27 linear solver in our windows code implementation to test its performances.

Finally, in terms of objective function one can observe that, since in cases with 1 and 2 scenarios large amount of wind power is injected

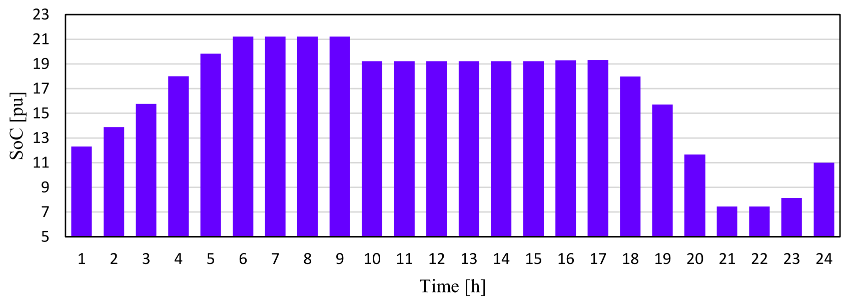

Fig. 9. SOC profile of ESS at node 1045 in scenario s1 and contingency in the connecting line between nodes 1041 and 1043.

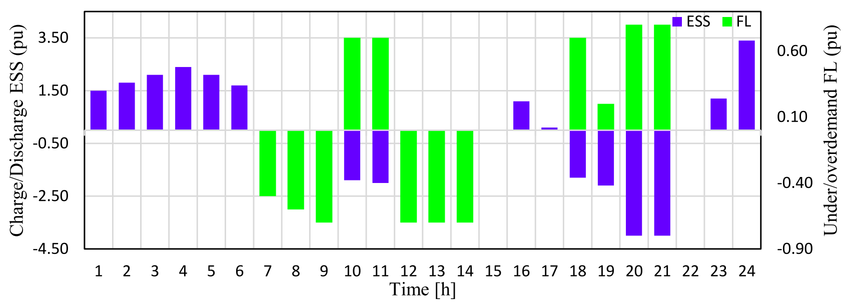

Fig. 10. Injection and absorption profile of active power for both ESS and FL and contingency in the connecting line between nodes 1041 and 1043.

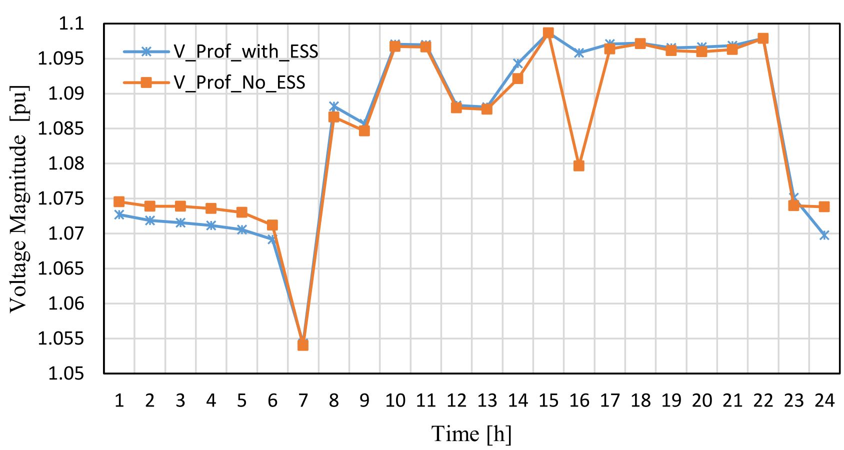

Fig. 11. Voltage magnitude of bus 1045 in contingency in the connecting line between nodes 1041 and 1043 for both with and without ESS cases.

into the system, generation curtailment occurs in peak hours which causes an increase in total cost for these two cases. Note that we initially generated 10 scenarios as in Fig. 4, and for the cases with larger numbers, the scenarios are replicated out of the original set of scenarios. For this reason the value of total cost remains unchanged for the cases with more than 10 scenarios.

3.2.3. Here and now vs. wait and see decisions

In this subsection comparative results are provided with the advocated single-stage S-MP-SCOPF with only W&S decisions and a two-stage S-MP-SCOPF problem with both H&N and W&S decisions (hereafter called as H&N option for brevity), see the extended formulation in Section 2.

When only W&S decisions are considered, the single-stage S-MP-SCOPF problem is decomposable by scenarios to obtain a series of deterministic multiperiod SCOPF (D-MP-SCOPF) models, as shown in Fig. 2 and, if parallel computations are implemented, computation efficiency can be improved significantly (i.e. $22,110/289 \approx 76$ times faster). This is illustrated for the Nordic32 test case by increasing parallel processors against total CPU time in Fig. 12.

Our additional results show empirically that two-stage S-MP-SCOPF model (both H&N and W&S decisions) is computationally slower (with IPOPT but necessarily with a tractable solution approach) than the single-stage S-MP-SCOPF model (only W&S decisions). Concretely, for 5 bus test system, the elapsed time is 20 s when only W&S decision variables are considered whereas the time rises to 227 s for the case when both H&N and W&S decision variables are considered. Similarly, for Nordic32 test case, the problem with 10 H&N generators is solved after 9481 s while the initial case with all decision variables as W&S was solved in 5985 s.

In this context, Fig. 13 illustrates the expected active generated power profile of the most expensive generator which acts as a W&S decision variable in both SCOPF models. It can be seen clearly that in the two-stage S-MP-SCOPF model (less degree of freedom), this expensive unit generates more active power as compared to the single-stage S-MP-SCOPF model (more degree of freedom) to cover the RES uncertainties.

Next remarkable observation in Nordic32 test system is that, although the total cost of H&N option is larger than the cost of W&S option (i.e., 288,274€ for H&N and 256,464€ for the W&S option), the

Table 10
Nordic32 test system results for different scenarios.

Number of scenarios	Total cost (€)	Continues variables	Constraints	Iter	Time (s)
1	555,874	197,206	287,596	123	289
2	421,924	394,582	575,192	144	764
3	652,595	591,788	862,788	167	1,404
4	319,122	789,164	1,150,384	173	2,040
5	297,430	986,540	1,437,980	160	2,283
6	284,137	1,183,916	1,725,576	166	2,878
7	274,769	1,381,292	2,013,172	171	3,596
8	267,411	1,578,668	2,300,768	169	4,100
9	261,006	1,776,044	2,588,364	180	4,451
10	256,464	1,973,420	2,875,960	186	5,985
20	256,464	3,312,280	5,751,920	185	14,351
30	256,464	4,968,420	8,627,880	186	22,110
40	IPOPT failed				

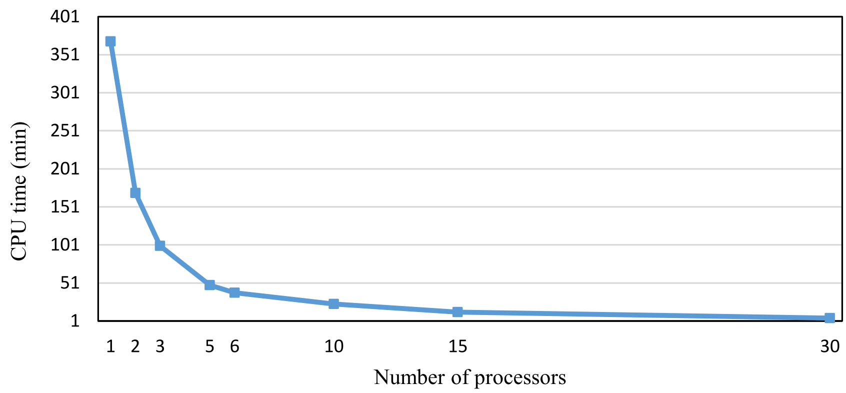

Fig. 12. Total CPU time with respect to different number of parallel processors.

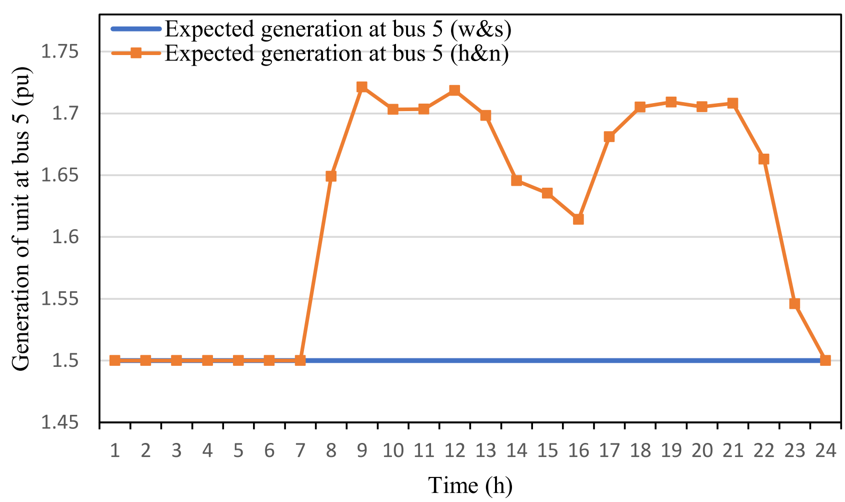

Fig. 13. Expected generation of unit at bus 5 in H&N and the corresponding expected value in W&S option in 5-bus test system.

value of active power generation profile of almost every H&N generator is lower than the expected values of the same units when considered as W&S decisions. Figs. 14 and 15 show this for buses 38 and 60 respectively. This implies that when both H&N and W&S variables are considered, H&N units generate less in order to allow fast responsive but more expensive W&S units to capture the RES uncertainties.

4. Conclusions and future work

The research efforts devoted to address the challenges of extending the state-of-the-art in AC SCOPF (i.e., deterministic and single time period) are scarce and mostly capture one novel feature at the time. This paper has extended the state-of-the-art in AC SCOPF to capture two new dimensions (RES stochasticity and multiple time periods) as well as to model time dependent constraints of emerging sources of flexibility (FL and ESS). Accordingly, this paper solves for the first time a new NLP problem formulation in the form of stochastic multi-period AC SCOPF (S-MP-SCOPF) which we envision for procuring flexibility for ancillary services (congestion and voltage control) in renewable supply dominated power systems of the future. This problem enables computing optimal set points of the flexibility resources and other conventional control means for congestion management and voltage control in day-ahead operation planning.

As we address a new problem, full problem details and results have been provided for a 5-node test system to foster benchmarking. The results obtained for this system show the effectiveness of the ESS and

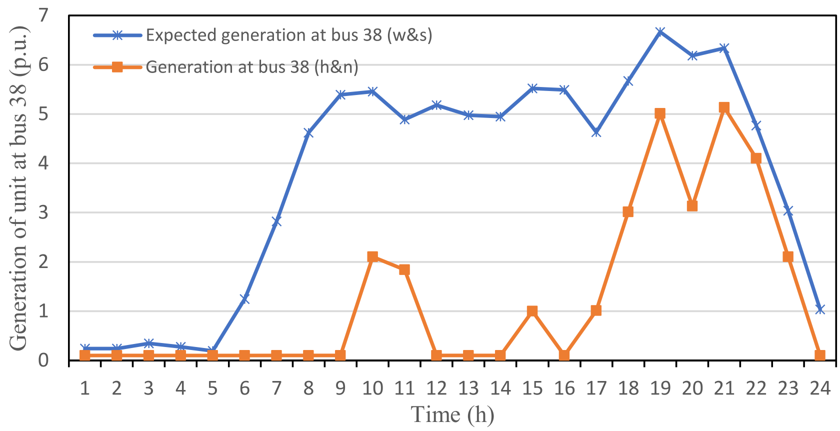

Fig. 14. Generation of unit at bus 38 in H&N and the expected corresponding value in W&S problem in Nordic32 test system.

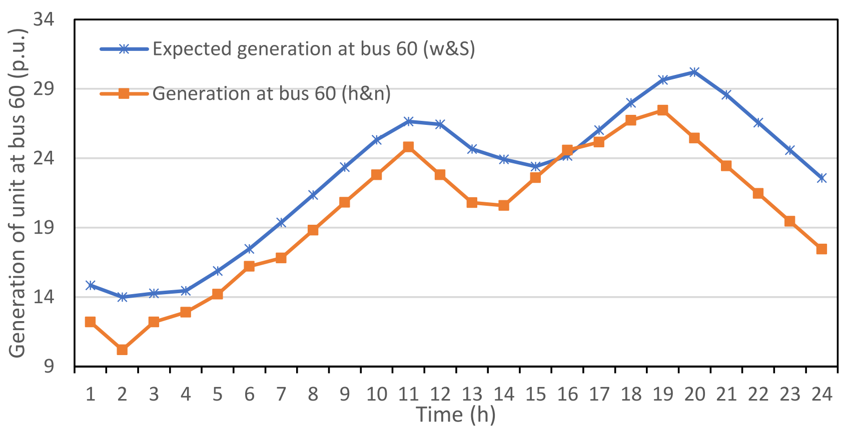

Fig. 15. Generation of unit at bus 60 in H&N and the expected corresponding value in W&S problem in Nordic32 test system.

FL for flexibility provision in day-ahead operation, which are able to reduce the load curtailment cost up to 90.5%.

The Nordic32 test system has been used to ascertain scalability, noting and as shown in Table 1 that scalability is rarely addressed by the few works that extend the state-of-the-art in AC SCOPF. The largest NLP S-MP-SCOPF problem solved in this work (60 nodes, 34 states, 24 time periods, 30 scenarios) is roughly equivalent in size to solving an AC OPF problem for a system of huge size (cca. 1,500,000 nodes). Very few works report results for such a big NLP problem. We have relied on the state-of-the-art NLP solver IPOPT, which is widely used to solve AC OPF/SCOPF problems. The running time obtained for the largest NLP problem on this system (roughly 5 millions optimization variables and 9 millions constraints, which is very close to the edge of computer/solver limit) is 22,110 s. While this time could be deemed a bit excessive for day-ahead operation planning, the elapsed time for a problem that includes three times less scenarios is 5,985 s, which is still acceptable. Furthermore, problem decomposition and parallel computations of single stage S-MP-SCOPF with only "wait and see" variables can greatly speed up the solution time with up to 76 times.

The paper has discussed that a massive reduction in computation time could be expected by using a more performant linear solver within IPOPT, a tailored implementation by parallelizing some computations [12], merely using a commercial solver, or by developing iterative methodologies [10].

This direct approach can thus scale to medium size systems by careful beforehand knowledge of problematic/binding contingencies, as an input from the operator, as well as reducing the number of uncertainty scenarios to a few.

As future work, we plan to develop a tractable approach of S-MP-SCOPF problem through decomposition and approximation along the above mentioned lines. Another research stream would be consideration of more agile corrective actions in case of contingencies in finer time resolutions to facilitate different ancillary service activation (i.e. particularly 10-minute and 30-minute reserves) if available from some ancillary service market clearing.

Finally, as the correlation among wind farms mimics the practical conditions more realistically, we also plan to address specifically this issue in our future work.

CRediT authorship contribution statement

Mohammad Iman Alizadeh: Conceptualization, Methodology, Software, Writing – original draft, Writing – review & editing, Investigation, Validation. **Muhammad Usman:** Methodology, Software, Writing – review & editing, Investigation. **Florin Capitanescu:** Conceptualization, Methodology, Writing - review & editing, Supervision, Funding acquisition, Project administration.

Declaration of competing interest

The authors declare that they have no known competing financial interests or personal relationships that could have appeared to influence the work reported in this paper.

Acknowledgement

This research work has received funding from the European Union's Horizon 2020 research and innovation program under grant agreement No. 864298 (project ATTEST).

References

[1] Balu Neal, Bertram Timothy, Bose Anjan, Brandwajn Vladimir, Cauley Gerry, Curtice David, et al. On-line power system security analysis. Proc IEEE 1992;80(2):262–82.

[2] Alizadeh MI, Moghaddam M Parsa, Amjady N, Siano P, Sheikh-El-Eslami MK. Flexibility in future power systems with high renewable penetration: A review. Renew Sustain Energy Rev 2016;57:1186–93.

[3] Wang Qin, Hodge Bri-Mathias. Enhancing power system operational flexibility with flexible ramping products: A review. IEEE Trans Ind Inf 2016;13(4):1652–64.

[4] Capitanescu Florin, Ramos JL Martinez, Panciatici Patrick, Kirschen Daniel, Marcolini A Marano, Platbrood Ludovic, et al. State-of-the-art, challenges, and future trends in security constrained optimal power flow. Electr Power Syst Res 2011;81(8):1731–41.

[5] Stott Brian, Alsaç Ongun. Optimal power flow: Basic requirements for real-life problems and their solutions. In: SEPOPE XII symposium, Vol. 11. Rio De Janeiro, Brazil; 2012.

[6] Capitanescu Florin. Challenges ahead risk-based AC optimal power flow under uncertainty for smart sustainable power systems. In: Dynamic vulnerability assessment and intelligent control: For sustainable power systems. John Wiley & Sons; 2018, p. 149.

[7] Capitanescu Florin, Glavic Mevludin, Ernst Damien, Wehenkel Louis. Applications of security-constrained optimal power flows. In: Proceedings of modern electric power systems symposium. 2006.

[8] Sharifzadeh Hossein, Amjady Nima, Zareipour Hamidreza. Multi-period stochastic security-constrained OPF considering the uncertainty sources of wind power, load demand and equipment unavailability. Electr Power Syst Res 2017;146:33–42.

[9] Phan Dzung, Kalagnanam Jayant. Some efficient optimization methods for solving the security-constrained optimal power flow problem. IEEE Trans Power Syst 2013;29(2):863–72.

[10] Platbrood Ludovic, Capitanescu Florin, Merckx Christian, Crisciu Horia, Wehenkel Louis. A generic approach for solving nonlinear-discrete security-constrained optimal power flow problems in large-scale systems. IEEE Trans Power Syst 2013;29(3):1194–203.

[11] Jiang Quanyuan, Xu Kai. A novel iterative contingency filtering approach to corrective security-constrained optimal power flow. IEEE Trans Power Syst 2013;29(3):1099–109.

[12] Kardoš Juraj, Kourounis Drosos, Schenk Olaf. Two-level parallel augmented schur complement interior-point algorithms for the solution of security constrained optimal power flow problems. IEEE Trans Power Syst 2019;35(2):1340–50.

[13] Avramidis Iason-Iraklis, Capitanescu Florin, Karagiannopoulos Stavros, Vrettos Evangelos. A novel approximation of security-constrained optimal power flow with incorporation of generator frequency and voltage control response. IEEE Trans Power Syst 2020.

[14] de Magalhães Carvalho Leonel, da Silva Armando Martins Leite, Miranda Vladimiro. Security-constrained optimal power flow via cross-entropy method. IEEE Trans Power Syst 2018;33(6):6621–9.

[15] Madani Ramtin, Ashraphijuo Morteza, Lavaei Javad. Promises of conic relaxation for contingency-constrained optimal power flow problem. IEEE Trans Power Syst 2015;31(2):1297–307.

[16] Yan M, Shahidehpour M, Paaso A, Zhang C, Abdulwhab A, Abusorrah A. A convex three-stage SCOPF approach to power system flexibility with unified power flow controllers. IEEE Trans Power Syst 2020;1.

[17] Valencia-Zuluaga Tomás, Agudelo-Martinez Daniel, Arango-Angarita Dario, Acosta-Urrego Camilo, Rivera Sergio, Rodríguez-Medina Diego, Gers Juan. A fast decomposition method to solve a security-constrained optimal power flow (SCOPF) problem through constraint handling. IEEE Access 2021;9:52812–24.

[18] Velloso Alexandre, Van Hentenryck Pascal, Johnson Emma S. An exact and scalable problem decomposition for security-constrained optimal power flow. Electr Power Syst Res 2021;195:106677.

[19] Weinhold R, Mieth R. Fast security-constrained optimal power flow through low-impact and redundancy screening. IEEE Trans Power Syst 2020;35(6):4574–84.

[20] Velay Maxime, Vinyals Meritxell, Besanger Yvon, Retière Nicolas. Fully distributed security constrained optimal power flow with primary frequency control. Int J Electr Power Energy Syst 2019;110:536–47.

[21] Karbalaei Farid, Shahbazi Hamidreza, Mahdavi Majid. A new method for solving preventive security-constrained optimal power flow based on linear network compression. Int J Electr Power Energy Syst 2018;96:23–9.

[22] Gazafroudi Amin Shokri, Neumann Fabian, Brown Tom. Topology-based approximations for N- 1 contingency constraints in power transmission networks. Int J Electr Power Energy Syst 2021;108:107–702.

[23] Velloso Alexandre, Van Hentenryck Pascal. Combining deep learning and optimization for preventive security-constrained DC optimal power flow. IEEE Trans Power Syst 2021.

[24] Capitanescu Florin, Fliscounakis Stéphane, Panciatici Patrick, Wehenkel Louis. Cautious operation planning under uncertainties. IEEE Trans Power Syst 2012;27(4):1859–69.

[25] You Lei, Ma Hui, Saha Tapan, Liu Gang. Risk-based contingency-constrained optimal power flow with adjustable uncertainty set of wind power. IEEE Trans Ind Inf 2021.

[26] Vrakopoulou Maria, Katsampani Marina, Margellos Kostas, Lygeros John, Andersson Göran. Probabilistic security-constrained AC optimal power flow. In: 2013 IEEE grenoble conference. IEEE; 2013, p. 1–6.

[27] Nycander E, Söder L. Comparison of stochastic and deterministic security constrained optimal power flow under varying outage probabilities. In: 2019 IEEE milan powerTech. 2019, p. 1–6.

[28] Venzke Andreas, Chatzivasileiadis Spyros. Convex relaxations of security constrained AC optimal power flow under uncertainty. In: 2018 Power systems computation conference. IEEE; 2018, p. 1–7.

[29] Hamon Camille, Perninge Magnus, Söder Lennart. The value of using chance-constrained optimal power flows for generation re-dispatch under uncertainty with detailed security constraints. In: 2013 IEEE PES Asia-Pacific power and energy engineering conference. IEEE; 2013, p. 1–6.

[30] Karangelos Efthymios, Wehenkel Louis. An iterative AC-SCOPF approach managing the contingency and corrective control failure uncertainties with a probabilistic guarantee. IEEE Trans Power Syst 2019;34(5):3780–90.

[31] Yang Linfeng, Zhang Chen, Jian Jinbao. A parallel method for solving the DC security constrained optimal power flow with demand uncertainties. Int J Electr Power Energy Syst 2018;102:171–8.

[32] Murillo-Sánchez Carlos E, Zimmerman Ray D, Anderson C Lindsay, Thomas Robert J. Secure planning and operations of systems with stochastic sources, energy storage, and active demand. IEEE Trans Smart Grid 2013;4(4):2220–9.

[33] Fuchs Alexander, Garrison Jared, Demiray Turhan. A security-constrained multi-period OPF for the locational allocation of automatic reserves. In: 2017 IEEE manchester powertech. IEEE; 2017, p. 1–6.

[34] Schanen Michel, Gilbert François, Petra Cosmin G, Anitescu Mihai. Toward multiperiod ac-based contingency constrained optimal power flow at large scale. In: 2018 Power systems computation conference. IEEE; 2018, p. 1–7.

[35] Cao Jun, Du W, Wang HF. An improved corrective security constrained OPF with distributed energy storage. IEEE Trans Power Syst 2015;31(2):1537–45.

[36] Wächter A, Biegler LT, Lang YD, Raghunathan A. IPOPT: An interior point algorithm for large-scale nonlinear optimization. 2002.

[37] Sharma Kailash Chand, Jain Prerna, Bhakar Rohit. Wind power scenario generation and reduction in stochastic programming framework. Electr Power Compon Syst 2013;41(3):271–85.

[38] Arthur David, Vassilvitskii Sergei. k-means++: The advantages of careful seeding. Technical report, Stanford; 2006.

[39] Gayme Dennice, Topcu Ufuk. Optimal power flow with large-scale storage integration. IEEE Trans Power Syst 2012;28(2):709–17.

[40] Shen Ziqi, Wei Wei, Wu Danman, Ding Tao, Mei Shengwei. Modeling arbitrage of an energy storage unit without binary variables. CSEE J Power Energy Syst 2020;7(1):156–61.

[41] Yong T, Entriken R, Zhang P. Reserve determination for system with large wind generation. In: 2009 IEEE power & energy society general meeting. IEEE; 2009, p. 1–7.

[42] Dunning Iain, Huchette Joey, Lubin Miles. JuMP: A modeling language for mathematical optimization. SIAM Rev 2017;59(2):295–320.

[43] Van Cutsem Thierry, Papangelis Lampros. Description, modeling and simulation results of a test system for voltage stability analysis. Technical report, université de Liège; 2013.

[44] Pena Ivonne, Martinez-Anido Carlo Brancucci, Hodge Bri-Mathias. An extended IEEE 118-bus test system with high renewable penetration. IEEE Trans Power Syst 2017;33(1):281–9.